Steel Fiber-Reinforced Concrete Panels in Shear: Analysis and Modeling

by Jimmy Susetyo, Paul Gauvreau, and Frank J. Vecchio

Finite element (FE) studies are undertaken to investigate the accuracy of currently available concrete constitutive models in predicting the behavior of steel fiber-reinforced concrete (SFRC) panels tested in pure shear. The tension-stiffening, tension-softening, and compression-softening behaviors of the panels are evaluated and compared with predictions made using the Disturbed Stress Field Model (DSFM) and currently available concrete constitutive models. In addition, the effects of crack slip and crack spacing parameters on the modeling accuracy are assessed.

The FE analysis results indicate that although current constitutive models are able to simulate the behavior of conventionally reinforced concrete panels accurately, the models overestimate the strength and deformation capacity of SFRC elements. Three factors are found to significantly influence the calculation accuracy: the tension stiffening/softening model, the consideration of shear slip on crack surfaces, and the crack spacing parameters.

Keywords: compression softening; crack slip; crack spacing; finite elements; panel tests; steel fiber; tension softening; tension stiffening.

INTRODUCTION

The effectiveness of steel fibers in enhancing the shear resistance of concrete has been demonstrated through a series of panel tests conducted by Susetyo[1] and Susetyo et al.[2] Two concrete panels containing conventional transverse reinforcement and eight concrete panels containing various amounts and types of hooked-end steel fibers were tested under in-plane pure shear loading. The test results indicate that steel fiber-reinforced concrete (SFRC) panels containing at least 1.0% of fibers by volume were able to achieve shear strengths and deformation capacities approximately equivalent to those attained from concrete panels containing conventional minimum shear reinforcement. Significant improvements in the postcracking principal tensile stress-strain response of the concrete were also observed, with strain-hardening behavior observed in panels containing at least 1.0% of fiber by volume.

In addition to demonstrating the ability of steel fibers to enhance the shear resistance of the concrete, the panel tests also allowed a more thorough investigation of SFRC behavior. Beyond what can be achieved from beam tests, the panel tests enabled the application of a constant and uniform shear-stress condition on the test specimens without the obscuring effects of flexure. Various aspects of concrete constitutive behavior, such as tension stiffening, tension softening, and compression softening could then be evaluated and compared with predictions made using currently available concrete constitutive models. This allowed for an evaluation of the accuracy of the current models in representing the behavior of SFRC.

This paper compares various aspects of the concrete behavior in SFRC panels tested by Susetyo et al.[2] to corresponding predictions of response made using available concrete constitutive models. The predictions were produced using a nonlinear finite element (FE) program based on the Disturbed Stress Field Model[3] (DSFM). The concrete behaviors compared include tension stiffening, tension softening, compression softening, crack slip, and crack spacing. Comparisons to the Variable Engagement Model, a tension-softening model for FRC elements subjected to uniaxial tensile stress proposed by Voo and Foster,[4] were also made. Discrepancies between the experimental results and the predictions are addressed and discussed.

RESEARCH SIGNIFICANCE

Assessments are made on the accuracy of currently available concrete constitutive models in simulating the behavior of SFRC panels; discrepancies between the calculated responses and the experimental results are addressed and discussed. This study aids in identifying deficiencies in current models and provides a better understanding of the factors influencing the accuracy of numerical analyses. In turn, these investigations will facilitate the development of improved constitutive models to more accurately simulate the behavior of SFRC. Ultimately, the newly developed constitutive models can be used to better design SFRC members.

CONSTITUTIVE RESPONSE OF SHEAR PANELS
Test panel details

Ten 35 x 35 x 2.75 in. (890 x 890 x 70 mm) panels were tested under in-plane pure-shear monotonic loading condition using the Panel Element Tester facility shown in Fig. 1. Two panels served as control specimens and were orthogonally reinforced with 40-D8 deformed wires in the longitudinal direction (ρ_x = 3.31%) and 10-D4 deformed wires in the transverse direction (ρ_y = 0.42%) (refer to Fig. 2(a)).

The remaining eight panels, containing steel fibers, were reinforced in the longitudinal direction only with 40-D8 deformed bars (ρ_x = 3.31%) (refer to Fig. 2(b)). Three types of hooked-end steel fibers (RC80/50-BN, RC80/30-BP, and RC65/35-BN) were used. In addition, three different fiber-volume contents (0.5, 1.0, and 1.5%) and two different concrete compressive strengths (7.3 and 11.6 ksi [50 and 80 MPa]) were investigated.

The properties of concrete and steel fibers are listed in Table 1. The concrete compressive strengths were obtained using uniaxial cylinder compression tests. Details of the

Jimmy Susetyo *is a Practicing Engineer at Hatch Mott MacDonald Limited, Mississauga, ON, Canada. He received his PhD in 2009 from the University of Toronto, Toronto, ON, Canada. His research interests include analysis and design of concrete structures, particularly fiber-reinforced concrete.*

Paul Gauvreau *is an Associate Professor of civil engineering at the University of Toronto. His research interests include the development of efficient structural systems for bridges using high-performance materials, especially high-performance concrete.*

Frank J. Vecchio, *FACI, is a Professor in the Department of Civil Engineering at the University of Toronto. He is a member of Joint ACI-ASCE Committee 441, Reinforced Concrete Columns, and 447, Finite Element Analysis of Reinforced Concrete Structures. His research interests include nonlinear analysis and design of reinforced concrete structures, constitutive modeling, performance assessment and forensic investigation, and repair and rehabilitation of structures.*

dry composition of the concrete mixtures and test programs can be found in Susetyo.[1] The properties of the reinforcing steel are listed in Table 2. The deformed wires, due to cold-forming, did not exhibit a yield plateau; their yield strength and yield strain were thus determined from the proportionality limit.

Analyses of test data

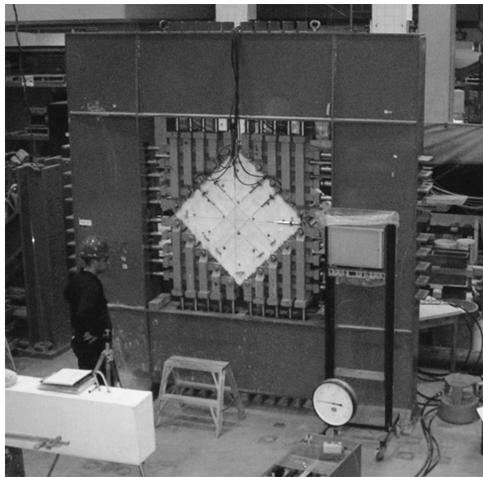Test data from the panels were acquired continuously from load cells, pressure transducers, linear variable differential transducers (LVDTs), and strain gauges through the course of each test. Mechanical strain gauge (Zurich gauge) readings and crack width measurements were taken at the conclusion of each load stage. The LVDT and Zurich gauge data provided average strain measurements in four directions: x-axis (longitudinal) direction, y-axis (transverse) direction, vertical direction (angled at 45 degrees with respect to the x-axis), and horizontal direction (angled
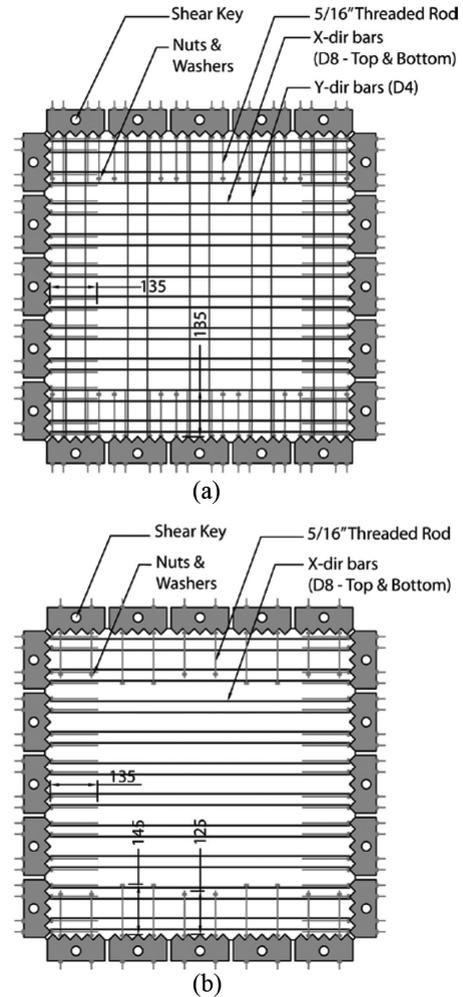

Fig. 2—Details of test specimens: (a) control panels; and (b) FRC panels.

Fig. 1—Panel element tester.

Table 1—Concrete and fiber properties used in experiments and FE modeling

ID	f_c', ksi (MPa)	ε_c', × 10⁻³	f_t', ksi (MPa)	E_c, ksi (GPa)	s_m, in. (mm)	V_f, %	l_f, in. (mm)	d_f, in. (mm)	f_{uf}, ksi (MPa)	τ_b, ksi (MPa)
C1C	9.53 (65.7)	2.410	0.387 (2.67)	5033 (34.7)	2.25 (57.2)*	—	—	—	—	—
C1F1V1	7.45 (51.4)	2.150	0.344 (2.37)	4699 (32.4)	4.50 (114.4)	0.5	2.0 (50)	0.025 (0.62)	152 (1050)	0.558 (3.85)
C1F1V2	7.75 (53.4)	2.670	0.350 (2.41)	3887 (26.8)	2.15 (54.7)	1.0	2.0 (50)	0.025 (0.62)	150 (1050)	0.563 (3.88)
C1F1V3	7.21 (49.7)	2.500	0.338 (2.33)	3945 (27.2)	2.25 (57.2)†	1.5	2.0 (50)	0.025 (0.62)	152 (1050)	0.554 (3.82)
C1F2V3	8.66 (59.7)	3.280	0.370 (2.55)	3438 (23.7)	1.50 (38.1)	1.5	1.20 (30)	0.015 (0.38)	334 (2300)	0.579 (3.99)
C1F3V3	6.60 (45.5)	2.340	0.323 (2.23)	3960 (27.3)	2.25 (57.2)	1.5	1.40 (35)	0.022 (0.55)	160 (1100)	0.541 (3.73)
C2C	13.13 (90.5)	2.700	0.455 (3.14)	5816 (40.1)	2.60 (66.2)*	—	—	—	—	—
C2F1V3	11.43 (78.8)	2.770	0.425 (2.93)	5062 (34.9)	1.42 (36.0)	1.5	2.0 (50)	0.025 (0.62)	152 (1050)	0.621 (4.28)
C2F2V3	11.10 (76.5)	2.220	0.419 (2.89)	6164 (42.5)	1.83 (46.6)	1.5	1.20 (30)	0.015 (0.38)	334 (2300)	0.616 (4.25)
C2F3V3	8.99 (62.0)	2.030	0.377 (2.60)	5714 (39.4)	1.60 (40.6)	1.5	1.40 (35)	0.022 (0.55)	160 (1100)	0.585 (4.03)

*For C1C-R, C2C, and analyses using VEM, $s_{mx} = s_{my} = 0$ (s_m is calculated automatically by VecTor2).
†For C1F1V3, three s_m were used in crack spacing evaluation: 2.25, 4.96, and 16.5 in. (57.2, 125.9, and 419.6 mm).
Note: $f_t' = 0.33 \times \sqrt{f_c'}$, and E_c is calculated according to Popovics base curve.[5]

at 135 degrees with respect to the x-axis). With the aid of a Mohr's circle diagram, all strain parameters, including principal compressive strain, principal tensile strain, shear strain, and orientation angle of the principal compressive strain, were then calculated. Knowing the strain parameters allowed the determination of the average stress parameters, such as reinforcement stresses f_{sx} and f_{sy} (calculated from the reinforcement average strain values using bare bar stress-strain relationships), concrete normal stresses f_{cx} and f_{cy} (calculated from equilibrium requirements using the known applied stresses on the panel and the calculated reinforcing bar stresses), concrete principal compressive stress f_{c2} and principal tensile stress f_{c1} (calculated using a Mohr's circle), and orientation angle of the principal stress field θ_σ (also from Mohr's circle). The reinforcement stresses were verified using the strains measured by the strain gauges. Details of the calculation procedures are presented in Susetyo.[1]

Discussions of the compression responses, tension responses, crack spacings, and crack widths are presented in the following. The discussions are based on the average panel deformations obtained from the LVDTs. The load-deformation responses, ultimate shear strengths, ductility, and failure modes of the test panels are discussed in detail by Susetyo et al.[2]
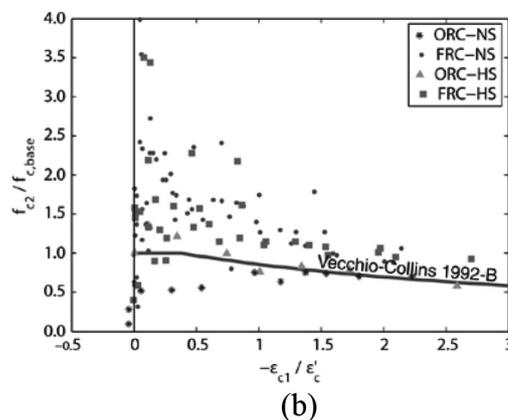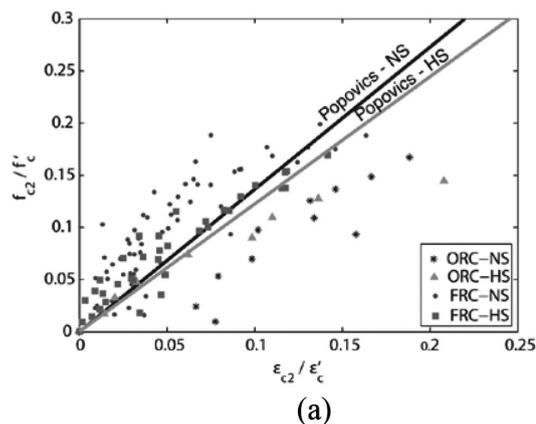
Compression response

Figure 3(a) plots the principal compressive stress-strain data obtained from the panels. The principal compressive stresses are normalized by the concrete compressive strength (f_c'), and the compressive strains are normalized by the concrete compressive strain corresponding to f_c'. Also plotted in Fig. 3(a) is the Popovics base-curve response.[5] It is clear that while there is much data scatter, owing to measurement inaccuracy arising from the very small principal compressive strains and stresses developed in the panels, the principal compressive stress-strain responses of the panels tended to follow the base curve. This endorses the widely held belief that fiber addition has only a minor influence, if any, on the pre-peak compressive stress response.[6,7] In addition, the FRC panels were also found to exhibit stiffer responses than the control panels.

In previous investigations, the compressive response of cracked reinforced concrete was found to be weaker and softer than the response of uniaxially compressed plain concrete due to the existence of transverse tensile strains and cracks[8]; the effect is known as compression softening. To investigate the compression-softening behavior in the FRC panels, the principal compressive stress data, normalized by the principal compressive stresses calculated using the Popovics base curve,[5] are plotted against $\varepsilon_{c1}/\varepsilon_c'$ in Fig. 3(b). Also plotted in the figure is the compression-softening model (1992-B Model) developed by Vecchio and Collins.[8] It can be observed that while the compression-softening model captures the degree of softening observed in the control panels reasonably well, the responses of the FRC panels indicated a significantly less softened behavior. It is likely that the fibers acted to limit and better control transverse cracking and tensile straining; hence, the compression-softening effect was reduced. However, the data exhibited a high degree of scatter and only small principal compressive stresses and strains were developed in the panels. A further investigation involving higher compressive stresses and strains is needed to clarify this issue.

Table 2—Reinforcement properties used in test panels and FE modeling

	x-direction	y-direction
Reinforcement ratio, %	3.31	0.42
Reinforcement diameter, in. (mm)	0.319 (8.10)	0.225 (5.72)
Reinforcement area, in.² (mm²)	0.08 (51.61)	0.04 (25.81)
Yield strength, ksi (MPa)	80.1 (552)	64.8 (447)
Yield strain, µε	2.58	2.41
Ultimate strength, ksi (MPa)	93.8 (647)	79.6 (549)
Elastic modulus, ksi (GPa)	32,590 (225)	27,151 (187)
Strain-hardening modulus, ksi (MPa)	322 (2219)	268 (1848)
Strain-hardening strain, µε	2.58	2.41

(a)

(b)

Note: ORC: conventionally reinforced concrete,
FRC: fiber reinforced concrete,
NS: fc' = 50 MPa (7.3 ksi)
HS: fc'= 80 MPa (11.6 ksi).

Vecchio-Collins 1992-B: $\dfrac{f_{c2}}{f_{c,bare}} = \dfrac{1}{1+0.27\left(\dfrac{-\varepsilon_{c1}}{\varepsilon_c'}-0.37\right)} \leq 1$

Fig. 3—(a) Principal compressive stress-strain response normalized against f_c' and ε_c'; and (b) compression-softening responses of panels.[8]

Tension response

Concrete post-cracking tensile behavior is thought to be governed by a combination of two phenomena: tension stiffening and tension softening. Tension stiffening describes the continuing ability of cracked concrete to carry tensile stresses between the cracks due to transfer of stresses

through bond between the reinforcement and the concrete. Tension softening, on the other hand, describes the existence of post-cracking tensile strength in the plain concrete.

Figure 4 plots the principal tensile stress-strain responses of the control panels. The principal tensile stresses are normalized by the principal tensile stress at which the first crack was observed in the panels. Also plotted in the figure is the Vecchio-Collins 1982 tension-stiffening model.[9] It is seen that the tensile behaviors of the control panels were accurately captured by the model.

In the FRC panels, tension softening is the dominant post-cracking tension mechanism—not tension stiffening. One of the most comprehensive constitutive models for tension softening in FRC elements subjected to uniaxial tensile stress is the Variable Engagement Model[4] (VEM). The VEM considers the tension softening of FRC as the sum of contribution of the fibers and the concrete matrix. The contribution of the fibers is given as follows[4]

$$f_{c1-fiber} = K_f \cdot K_d \cdot \frac{l_f}{d_f} \cdot V_f \cdot \tau_b \qquad (1)$$

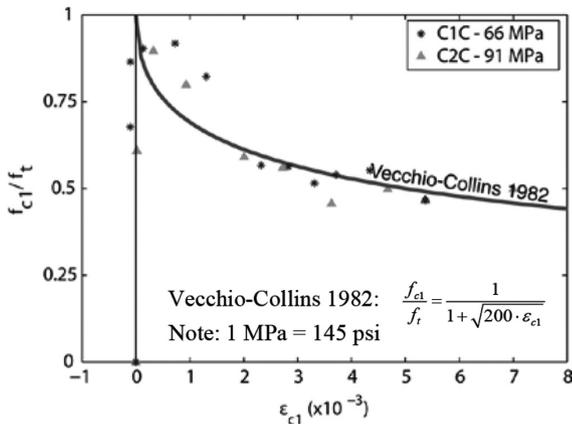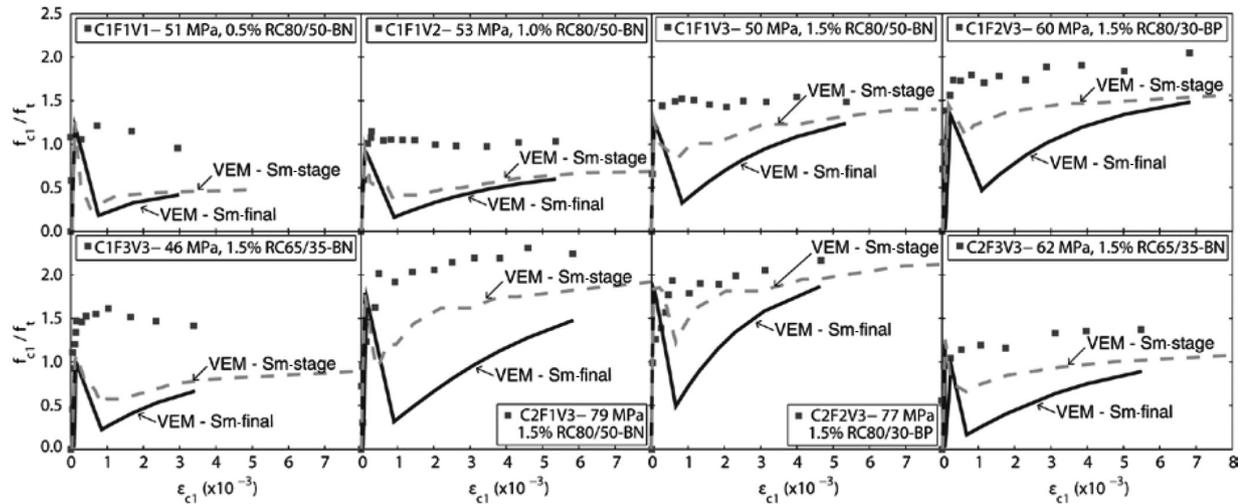$$K_f = \frac{\tan^{-1}\left(w_m/\alpha\right)}{\pi} \cdot \left(1 - \frac{2 \cdot w_m}{l_f}\right)^2 \qquad (2)$$

Fig. 4—Tensile-stiffening responses of control panels.

$$\alpha = d_f/3.5 \qquad (3)$$

in which l_f is the fiber length; d_f is the fiber diameter; V_f is the fiber-volume content; τ_b is the mean shear stress between the fibers and the concrete ($\tau_b = 2.5 \times f_t'$); w_m is the crack width; and K_d is fiber efficiency factor. The contribution of the concrete matrix is estimated using a linear relationship recommended by Wong and Vecchio[10] as follows

$$f_{c1-matrix} = f_{cr} \cdot \left[1 - \frac{\varepsilon_{c1} - \varepsilon_{cr}}{\varepsilon_{ch} - \varepsilon_{cr}}\right] \geq 0 \quad \text{for } \varepsilon_{cr} \leq \varepsilon_{c1} \qquad (4)$$

$$\varepsilon_{ch} = \frac{2 \cdot G_f}{f_{cr} \cdot s_m/2}; \quad 1.1\varepsilon_{cr} \leq \varepsilon_{ch} \leq 10\varepsilon_{cr} \qquad (5)$$

in which G_f is the fracture energy (assumed to be 75 N/m [0.43 lb/in.]); and ε_{ch} is the characteristic strain of the tensile softening curve (that is, the strain at which tensile stress becomes zero).

The normalized principal tensile stress-strain responses of the FRC panels are plotted in Fig. 5 together with the responses predicted by the VEM. The VEM calculations are based on crack widths as the controlling parameter; hence, the relationship between tensile strain ε_{c1} and crack width w_m is established using $w_m = \varepsilon_{c1} \cdot s_m$, in which s_m is the crack spacing. Two VEM curves are plotted in Fig. 5. The VEM-$S_{m-final}$ response curve was calculated using the average final crack spacing obtained from the experiment results (refer to Table 1), whereas the VEM-$S_{m-stage}$ curve was calculated using the average crack spacing corresponding to the crack widths used in the calculation (refer to Susetyo[1]). As is evident from the figure, the postcracking responses predicted by the VEM were overly conservative and the VEM underestimated the postcracking secant stiffness of the principal tensile stress response of the panels. It is also evident that the crack spacing parameter used in predicting the tensile behavior significantly influenced the prediction results. Thus, the tension-softening response in

Note: 1 MPa = 145 psi

Fig. 5—Tension-softening responses of FRC panels.

Table 3—Average final crack spacings of panels calculated using various methods

Panel ID	l_f/d_f	f_{cr},* ksi (MPa)	f_{res},* ksi (MPa)	$s_{m\text{-}exp}$, in. (mm)	$s_{m\text{-}RILEM}$†,in. (mm)	$s_{m\text{-}Moffatt}$,‡ in. (mm)
C1C	—	0.590 (4.07)	—	2.25 (57.2)	3.89 (98.9)	3.89 (98.9)
C1F1V1	81	0.550 (3.79)	0.167 (1.15)	4.50 (114)	2.41 (61.1)	2.71 (68.9)
C1F1V2	81	0.502 (3.46)	0.315 (2.17)	2.15 (54.7)	2.41 (61.1)	1.45 (36.9)
C1F1V3	81	0.629 (4.34)	0.415 (2.86)	2.25 (57.2)	2.41 (61.1)	1.33 (33.7)
C1F2V3	79	0.569 (3.92)	0.363 (2.50)	1.50 (38.1)	2.46 (62.6)	1.41 (35.8)
C1F3V3	64	0.690 (4.76)	0.338 (2.33)	2.25 (57.2)	3.04 (77.3)	1.99 (50.5)
C2C	—	0.599 (4.13)	—	2.61 (66.2)	3.89 (98.9)	3.89 (98.9)
C2F1V3	81	0.679 (4.68)	0.316 (2.18)	1.42 (36.0)	2.41 (61.1)	2.08 (52.9)
C2F2V3	79	0.627 (4.32)	0.389 (2.68)	1.83 (46.6)	2.46 (62.6)	1.48 (37.5)
C2F3V3	64	0.560 (3.86)	0.329 (2.27)	1.60 (40.6)	3.04 (77.3)	1.61 (40.8)

*Data obtained from uniaxial tension tests.
†RILEM formulation: $s_m = (50 + 0.25 \cdot k_1 \cdot k_2 \cdot d_b/\rho_{eff})[50/(l_f/d_f)]$.
‡Moffatt's formulation: $s_m = (50 + 0.25 \cdot k_1 \cdot k_2 \cdot d_b/\rho_{eff})[1 - f_{res}/f_{cr}]$.
Note: $d_b = 8.1$ mm; $\rho_{eff} = 3.31\%$; $k_1 = 0.8$ (deformed bars) or 1.6 (plain bars); $k_2 = (\varepsilon_1 + \varepsilon_2)/(2 \times \varepsilon_1)$.

FRC elements subjected to shear is substantially different than that manifested in uniaxially stressed elements, and additional development of a suitable constitutive model is required. Note that the lower response of the VEM-$S_{m\text{-}final}$ curves than that of the VEM-$S_{m\text{-}stage}$ curves is due to the lower K_f values calculated for the VEM-$S_{m\text{-}final}$ curves than those calculated for the VEM-$S_{m\text{-}stage}$ curves for the evaluated range of tensile strains.

Crack spacing and crack widths

A commonly used method in relating average crack width to tensile strain in a concrete member is to express the crack width as a product of concrete tensile strain and the average final crack spacing (that is, $w_m = \varepsilon_{c1} \cdot s_m$), as was done previously. Because the fibers in FRC are found to bridge cracks and provide better crack propagation control as indicated by the reduced crack widths and spacings,[1,2] a model for average crack spacing specific to FRC elements is required.

To obtain better estimates of the average crack spacing in FRC members, Dupont and Vandewalle[11] (RILEM TC162) modified the average crack spacing expression used in Eurocode 2[12] by applying the multiplier $[50/(l_f/d_f)]$. Moffatt[13] proposed a similar modification to the Eurocode 2 model, using the modification factor $(1 - f_{res}/f_{cr})$ to account for the fiber contribution; f_{res} and f_{cr} are the postcracking residual tensile strength and the cracking tensile strength of the FRC member, respectively.

Table 3 lists the values of the crack spacing calculated using the models proposed by RILEM and by Moffatt.[13] The residual tensile strength f_{res} used in Moffatt's[13] formulation was obtained from uniaxial tension tests and was calculated as the average of the residual tensile strength at a crack opening of 1 and 3 mm (0.04 and 0.12 in.). Details of the uniaxial tension tests can be found in Susetyo.[1] For the control panels, which contained no fibers, the average crack spacings were calculated using the Eurocode 2 formulation.

It can be observed in Table 3 that the crack spacings calculated using the RILEM model were typically greater than the final spacings measured on the test panels. Note that the RILEM model only considers the fiber aspect ratio and, hence, it does not recognize the important influence of fiber content on the crack control characteristics of an FRC member. The crack spacing predictions calculated using the Moffatt[13] model yielded better results, as the model uses the postcracking residual tensile strength to account for fiber contribution in reducing the crack spacing. However, for most panels, Moffatt's[13] model produced smaller crack spacings than those measured during the tests, as indicated in Table 3.

A model to estimate the postcracking residual tensile strength and the first-cracking tensile strength is a necessity if accurate calculations of the crack spacing are to be achieved. Moreover, the crack spacings observed in the test panels showed a consistent progression toward lower values as the loading increased, with the final spacings being significantly less than those at intermediate load stages. Because the concrete stiffening/softening calculations, such as with the VEM, depend on crack widths and, thus, crack spacings, a model that can accurately represent crack spacing progression is required. No such model exists.

FE MODELING AND RESULTS
FE model details

For each of the panels tested, modeling was performed using VecTor2,[14] a nonlinear FE program based on the DSFM.[3] The primary objective was to investigate the accuracy of current constitutive models in predicting the behavior of FRC. For one specimen, Panel C1F1V3 ($V_f = 1.5\%$, $l_f = 2.0$ in. [50 mm], $l_f/d_f = 80$, $f_c' = 7.21$ ksi [49.7 MPa]), additional analyses were performed using three different crack spacings (2.25, 4.96, and 16.5 in. [57.2, 126, and 420 mm]) and using a constant rotation lag model to investigate the influence of crack spacing and crack slip on the modeling accuracy.

Given the uniformity of the structural properties and stress condition within each panel, the panels were modeled using a single four-noded plane stress rectangular element with dimensions of 35 x 35 x 2.76 in. (890 x 890 x 70 mm). The element was restrained against movement in the x- and y-directions at the lower left corner and against movement in the y-direction at the lower right corner, as illustrated in Fig. 6. The element was loaded in pure shear, with the load applied as a monotonically increasing load at the corners of the element.

The properties of the concrete and the steel fibers are listed in Table 1, and the properties of the conventional

reinforcement are given in Table 2. The bonded conventional reinforcement was modeled as smeared reinforcement embedded within the concrete element. For the control panels (Panel C1C and C2C), the smeared reinforcement was provided in both the x- and y-directions, whereas for the FRC panels, it was provided in the x-direction only.

To capture the behavior of the panels accurately, it was necessary to consider various influencing mechanisms in the VecTor2 analyses. Table 4 lists the mechanisms considered and the constitutive models selected to model these behaviors; a detailed description and discussion of these models is provided by Wong and Vecchio.[10] Particular attention was given to the tension-softening behavior, as it influences how the fiber reinforcement is modeled. Two types of tension-softening behaviors were considered: 1) a custom tension softening model, input by the user based on responses measured from standard material tests; and 2) the common linear decay tension-softening model, used in conjunction with VEM.

The custom tension-softening model was applied by specifying four points representing the postcracking tensile stress-strain relationship of the concrete. In this FE modeling, the tensile stress-strain relationships were derived from uniaxial
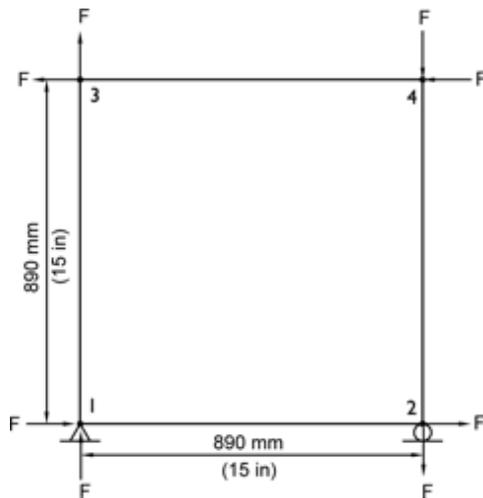

Fig. 6—FE model of panels.

tension tests conducted by Susetyo.[1] The final crack spacing measured during the tests was also input to prevent calculation of large crack spacing resulting from the absence of transverse reinforcement. When the linear tension-softening model was used in conjunction with VEM, the resulting tension-softening stresses were taken as the sum of those calculated using the linear tension-softening model for the plain concrete and those calculated using the VEM. The crack spacing was calculated automatically using Eq. (6) to (10).

Prediction of control specimens

The FE analysis results for the control specimens (Panels C1C and C2C) are shown in Fig. 7 and summarized in Table 5. As indicated in Fig. 7, the behavior of the control specimens was simulated reasonably accurately. The predicted ultimate shear capacities were conservative but generally within acceptable limits given the shear-critical nature of the specimens. Moreover, the FE modeling predicted the same failure mode due to the yielding of the transverse reinforcement, as observed in the experiments. Also, in conformity to the experiment results, the predicted concrete principal compressive stress and longitudinal reinforcement stress were below their maximum strength values, indicating neither concrete crushing nor longitudinal reinforcement yielding occurred. The predicted responses, however, terminated at a lower shear stress and strain than the experimental responses. This was largely due to the idealized multi-linear strain-hardening behavior assumed for the reinforcement; the actual reinforcement, being cold-drawn, did not possess a defined yield plateau and instead exhibited a pronounced strain-hardening behavior immediately following the limit of proportionality.

Prediction using custom tension-softening input

The FE analysis results for the FRC specimens analyzed using the custom tension-softening input are shown in Fig. 8 and summarized in Table 6. It is evident that the FE modeling using the constitutive models listed in Table 4 significantly overestimated the strength and deformation capacity of the FRC specimens, with the ratio of the calculated to measured shear strength having a mean of 1.275.

Table 4—Concrete constitutive models used in FE modeling

Behavior	Constitutive model used	Behavior	Constitutive model used
Compression pre-peak	Popovics (HSC)	Confined strength	Kupfer/Richart model
Compression post-peak	Modified Park-Kent	Dilatation	Variable Kupfer
Compression softening	Vecchio-1992A	Cracking criterion	Mohr-Coulomb (Stress)
Tension stiffening	Modified Bentz 2003	Crack slip check	Vecchio-Collins 1986
Tension softening	Custom input/linear + VEM	Crack width check	Agg/5 max crack width
Tension splitting	Not considered	Slip distortion	Vecchio-Lai/Vecchio-Lai + constant rotation

Table 5—Summary of FE analysis results: control specimens

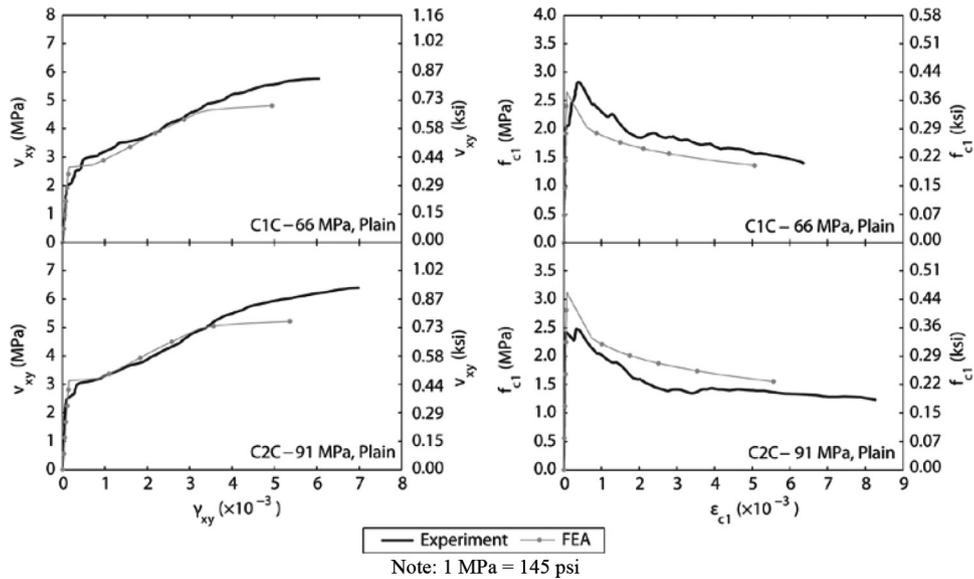| Panel ID	γ_u pred./ exp., $\mu\varepsilon$	v_u pred./ exp., psi (MPa)	$f_{c1\text{-}max}$ pred./ exp., psi (MPa)	$f_{c2\text{-}max}$ pred./ exp., psi (MPa)	$f_{sx\text{-}final}$ pred./ exp., ksi (MPa)	$f_{sy\text{-}final}$ pred./ exp., ksi (MPa)	w_m pred./exp., in. (mm)	s_m pred./ exp., in. (mm)	$v_{ci\text{-}pred}$, ksi (MPa)	$\delta_{s\text{-}pred}$, in. (mm)	$v_{u\text{-}pred}/ v_{u\text{-}exp.}$
C1C	4.94 6.01	699/837 (4.82/5.77)	384/416 (2.65/2.87)	–1307/–1697 (–9.01/–11.70)	25.2/36.2 (174/250)	65.3/72.7 (450/501)	0.029/0.022 (0.73/0.55)	5.67/2.24 (144/57)	–0.078 (–1.99)	–0.008 (–0.20)	0.835
C2C	5.36 7.00	757/928 (5.22/6.40)	454/370 (3.13/2.55)	–1413/–2107 (–9.74/–14.53)	27.4/49.5 (189/341)	65.4/74.3 (451/512)	0.032/0.020 (0.81/0.50)	5.71/2.60 (145/66)	–0.091 (–2.32)	–0.009 (–0.22)	0.816

Note: 1 MPa = 145 psi

Fig. 7—Comparison of observed and calculated responses of control specimens.

Table 6—Summary of FE analysis results: FRC specimens with Custom Tension Softening Model

Panel ID	γ_u pred. exp., $\mu\varepsilon$	v_u pred./exp., psi (MPa)	$f_{c1\text{-}max}$ pred./ exp., psi (MPa)	$f_{c2\text{-}max}$ pred./exp., psi (MPa)	$f_{sx\text{-}final}$ pred./ exp., ksi (MPa)	w_m pred./ exp., in. (mm)	s_m* pred./ exp., in. (mm)	$v_{ci\text{-}pred.}$, ksi (MPa)	$\delta_{s\text{-}pred.}$, in. (mm)	$v_{u\text{-}pred}/$ $v_{u\text{-}exp.}$
C1F1V1	8.82/2.77	0.521/0.512 (3.59/3.53)	0.463/0.410 (3.19/2.83)	−1.479/−0.976 (−10.20/−6.73)	39/22 (271/148)	0.062/0.022 (1.58/0.55)	4.50/4.50 (114/114)	0 (0)	0 (0)	1.017
C1F1V2	15.95/5.27	0.940/0.750 (6.48/5.17)	0.526/0.441 (3.63/3.04)	−2.464/−1.372 (−16.99/−9.46)	64/29 (441/201)	0.050/0.018 (1.27/0.45)	2.15/2.15 (54.7/54.7)	0 (0)	0 (0)	1.253
C1F1V3	20.70/5.10	1.127/0.779 (7.77/5.37)	0.625/0.454 (4.31/3.13)	−2.785/−1.407 (−19.20/−9.70)	73/30 (501/204)	0.064/0.018 (1.63/0.45)	2.25/2.25 (57.2/57.2)	0 (0)	0 (0)	1.447
C1F2V3	17.33/6.20	1.220/0.969 (8.41/6.68)	0.611/0.564 (4.21/3.89)	−2.973/−1.758 (−20.50/−12.12)	75/37 (517/256)	0.035/0.018 (0.90/0.45)	1.50/1.50 (38.1/38.1)	0 (0)	0 (0)	1.259
C1F3V3	11.37/4.27	1.041/0.811 (7.18/5.59)	0.701/0.558 (4.83/3.85)	−2.326/−1.468 (−16.04/−10.12)	56/31 (389/213)	0.033/0.020 (0.83/0.50)	2.25/2.25 (57.2/57.2)	0 (0)	0 (0)	1.284
C2F1V3	12.86/5.25	1.186/1.000 (8.18/6.90)	0.679/0.531 (4.68/3.66)	−2.802/−2.006 (−19.32/−13.83)	70/46 (480/315)	0.024/0.028 (0.62/0.70)	1.42/1.42 (36.0/36.0)	0 (0)	0 (0)	1.186
C2F2V3	16.12/4.35	1.250/0.915 (8.62/6.31)	0.674/0.544 (4.65/3.75)	−3.075/−1.559 (−21.20/−10.99)	79/32 (544/224)	0.041/0.026 (1.05/0.65)	1.84/1.84 (46.6/46.6)	0 (0)	0 (0)	1.366
C2F3V3	16.05/4.97	1.123/0.808 (7.74/5.57)	0.573/0.425 (3.95/2.93)	−2.795/−1.559 (−19.27/−10.75)	72/35 (496/238)	0.036/0.024 (0.92/0.60)	1.60/1.60 (40.6/40.6)	0 (0)	0 (0)	1.390

*s_m was input into VecTor2 and taken as final crack spacing measured during experiment.

It is believed that the stronger calculated responses were influenced by three factors. The first factor is the possible dissimilarity in fiber orientation between the panels and the uniaxial (dog-bone) tension test specimens, from which the tension softening models used were derived. In the FRC panels, the dense longitudinal reinforcement present may possibly have led to the fibers being oriented more in line with the direction of the longitudinal reinforcement, resulting in a reduced tensile strength in the principal tensile stress direction. In contrast, due to the smaller cross-sectional dimensions of the dog-bone test specimens, the probability of the fibers being oriented in the direction of the applied load was greater, particularly in specimens containing a high amount of fibers or long fibers. This aligned orientation may have resulted in an increased uniaxial tensile strength. As the custom tension-softening model used the tensile stress-strain relationships obtained from the uniaxial tension tests, the higher tensile strengths would result in the higher predicted panel responses.

The second factor relates to the different behavior between FRC with and without conventional steel reinforcement. The steel reinforcement provides additional crack control capability, resulting in smaller crack widths and crack spacings than if no steel reinforcement is provided. For FRC containing conventional reinforcement, when the contribution of the steel reinforcement is subtracted from the tensile response, the resulting concrete tension-softening behavior will be weaker than that in FRC without steel reinforcement because the smaller crack widths lead to fewer fibers being engaged in carrying the tensile stress. Therefore, the use of the tensile stress-strain relationships obtained from uniaxial tension tests will result in an overestimation of the predicted tensile stresses in the panels and, as a result, an overestimation of the predicted strength of the panels.

The third factor lies in the method by which the concrete principal tensile stresses and the shear slip are calculated. In the formulation of the DSFM, the concrete average post-cracking tensile stress is determined as the maximum of the
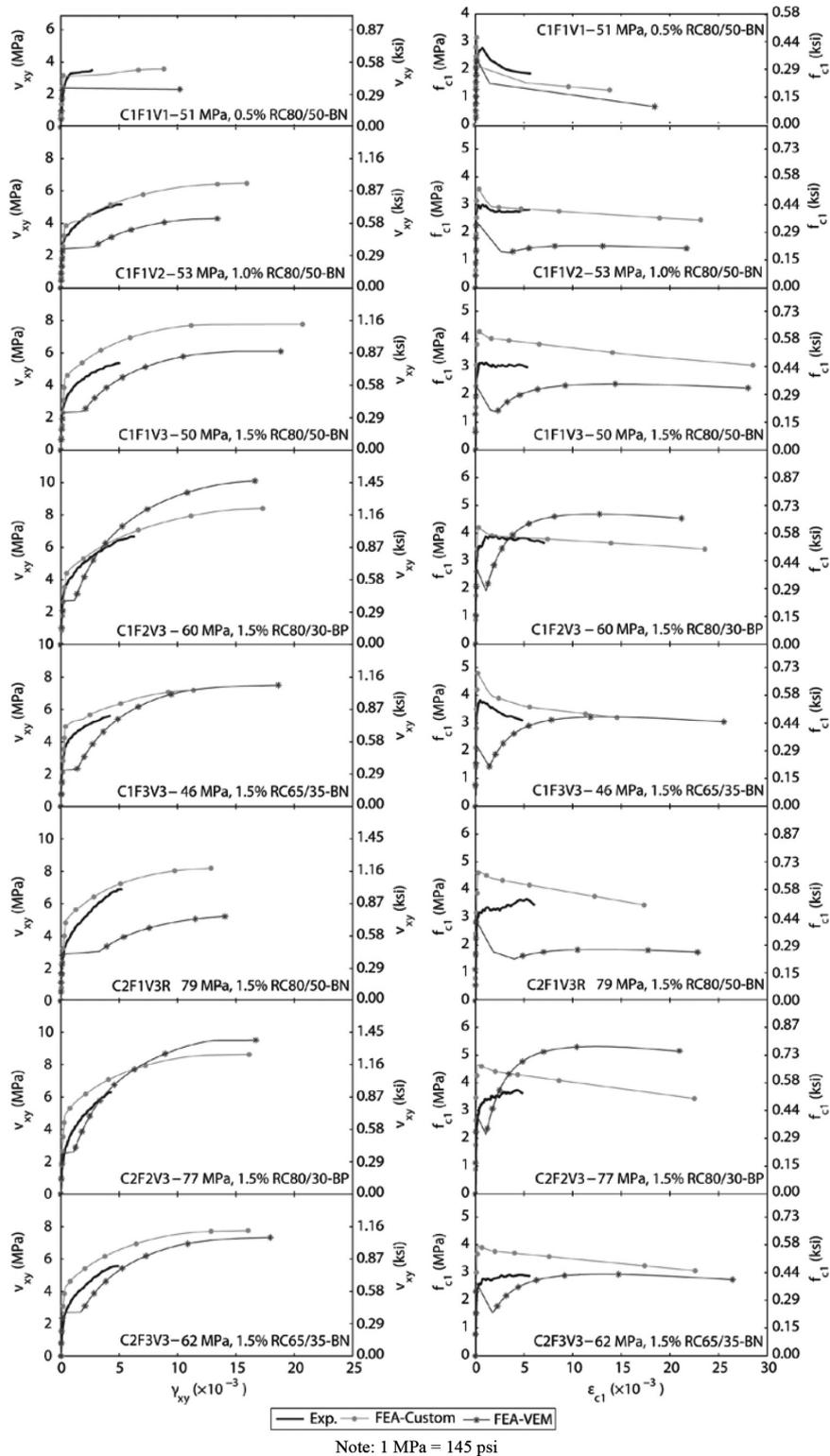
Fig. 8—Comparison of observed and calculated responses of FRC specimens.

stresses calculated from the tension-stiffening and tension-softening models. In an FRC element, the fibers will bridge the cracks, thereby significantly increasing the ability of the concrete to transmit tensile stresses across the cracks (that is, through tension softening) without any increase in the local reinforcement stresses. No local shear stresses arise at the crack and, hence, no failure due to crack slip will occur. The element will continue to carry the applied load until another failure mechanism—either the crushing of the concrete or

the yielding of the x-direction reinforcement—takes place. This was observed in the predicted responses, in which zero crack slips were predicted in all FRC panels, and where all analyses terminated with the concrete principal compressive stress reaching the peak compressive stress and/or the x-direction reinforcement yielding. These were incorrect, as the experiments indicated that crack slips occurred in all FRC panels and that the failure mode of all FRC panels was governed by the aggregate interlock failure.

Table 7—Summary of FE analysis results: FRC specimens with VEM

Panel ID	γ_u pred. exp., $\mu\epsilon$	v_u pred./exp., psi (MPa)	$f_{c1\text{-}max}$ pred./exp., psi (MPa)	$f_{c2\text{-}max}$ pred./exp., psi (MPa)	$f_{sx\text{-}final}$ pred./exp., ksi (MPa)	w_m pred./exp., in. (mm)	s_m pred./exp., in. (mm)	$v_{ci\text{-}pred.}$, ksi (MPa)	$\delta_{s\text{-}pred.}$, in. (mm)	$v_{u\text{-}pred}/v_{u\text{-}exp.}$
C1F1V1	10.19/2.77	0.338/0.512 (2.33/3.53)	0.345/0.410 (2.39/2.83)	–1.009/–0.976 (–6.96/–6.73)	33/22 (226/148)	0.124/0.022 (3.15/0.55)	6.73/4.50 (171/114)	0 (0)	0.0004 (–0.01)	0.660
C1F1V2	13.41/5.27	0.621/0.750 (4.28/5.17)	0.350/0.441 (2.41/3.04)	–1.839/–1.372 (–12.68/–9.46)	50/29 (346/201)	0.087/0.018 (2.20/0.45)	3.98/2.15 (101/54.7)	0 (0)	0 (0)	0.828
C1F1V3	18.85/5.10	0.885/0.779 (6.10/5.37)	0.345/0.454 (2.38/3.13)	–2.350/–1.407 (–16.20/–9.70)	64/30 (439/204)	0.086/0.018 (2.19/0.45)	3.07/2.25 (78.1/57.2)	0 (0)	0 (0)	1.136
C1F2V3	16.65/6.20	1.466/0.969 (10.11/6.68)	0.680/0.564 (4.69/3.89)	–3.263/–1.758 (–22.50/–12.12)	79/37 (543/256)	0.050/0.018 (1.26/0.45)	2.34/1.50 (59.5/38.1)	0 (0)	0 (0)	1.513
C1F3V3	18.64/4.27	1.086/0.811 (7.49/5.59)	0.467/0.558 (3.22/3.85)	–2.645/–1.468 (–18.24/–10.12)	67/31 (464/213)	0.073/0.020 (1.85/0.50)	2.85/2.25 (72.3/57.2)	0 (0)	0 (0)	1.340
C2F1V3	14.06/5.25	0.757/1.000 (5.22/6.90)	0.419/0.531 (2.89/3.66)	–2.255/–2.006 (–15.55/–13.83)	60/46 (417/315)	0.071/0.028 (1.80/0.70)	3.09/1.42 (78.6/36.0)	0 (0)	0 (0)	0.757
C2F2V3	16.70/4.35	1.610/0.915 (11.10/6.31)	0.770/0.544 (5.31/3.75)	–3.394/–1.559 (–23.40/–10.99)	80/32 (553/224)	0.049/0.026 (1.24/0.65)	2.34/1.84 (59.4/46.6)	0 (0)	0 (0)	1.759
C2F3V3	17.94/4.97	1.059/0.808 (7.30/5.57)	0.426/0.425 (2.94/2.93)	–2.795/–1.559 (–19.27/–10.75)	73/35 (504/238)	0.076/0.024 (1.92/0.60)	2.86/1.60 (72.7/40.6)	0 (0)	0 (0)	1.311

Prediction using variable engagement model

The FE analysis results for the FRC specimens analyzed using the VEM are also shown in Fig. 8 and are summarized in Table 7. Similar to the analyses using the custom tension-softening model, significant overestimation of the deformation capacity of the panels was observed. In terms of strength, the FE analyses overestimated the strength of panels containing short fibers (Panel C1F2V3, C1F3V3, C2F2V3, and C2F3V3) but underestimated the strength of the panels containing long fibers (Panel C1F1V1, C1F1V2, C1F1V3, and C2F1V3). The mean of the ratio of the predicted shear strength to the experimental shear strength was 1.163.

The VEM requires a certain amount of fiber slip to occur first before the fibers can be fully engaged in carrying the tensile stress. As a result, when the concrete cracks, a decline in the postcracking tensile stress is immediately observed, as fiber slip has not yet occurred. This causes a sudden increase in the reinforcement stress and a sudden opening of the crack, resulting in the plateau observed in the shear-stress, shear-strain responses plotted in Fig. 8. Immediately after, fiber slip occurs and the fibers become fully engaged in carrying the tensile load. This results in the subsequent ability of the panels to withstand additional loads.

Three parameters were found to significantly influence the VEM calculations: the matrix tensile strength, the crack spacing parameters, and the engagement parameter α. An increase in the tensile strength of the matrix will result in a stronger interfacial bond between the fibers and the concrete and, thus, an increase in the predicted tensile strength of the composite. Changing the crack spacing parameters was found to alter the predicted response significantly, as it affects the tensile response of the concrete. Detailed discussion of the crack spacing parameters will be given in the discussion that follows. The engagement parameter α reflects the resistance against slip between the fibers and the concrete matrix. The use of a low value of α resulted in fibers being engaged sooner and, thus, a higher tensile strength being achieved. Therefore, to obtain an accurate prediction of the response of an FRC element, an appropriate value of α should be used.

Similar to the analyses conducted using the custom tension-softening model, fe analyses conducted using the VEM-based tension softening, except for Panel C1F1V1, also terminated due to the concrete principal compressive stress reaching the peak compressive stress and/or due to yielding of the x-direction reinforcement. No crack slip was predicted for all FRC panels, except Panel C1F1V1, for the same reasons previously discussed.

DISCUSSION

The analysis results indicate that crack spacing has a significant influence on the accuracy of the predictions, as does the lack of crack slip and local shear stress on the crack interfaces. Additional analyses were therefore performed to evaluate the influence of these parameters on the accuracy of the modeling.

Influence of crack spacing parameters

It should be understood that, in a typical FRC element and particularly in those with sufficient fiber-volume ratio to exhibit tension-hardening response, the average crack spacing changes as additional cracks develop. Although the final crack spacing is generally used in FE modeling, it may result in an overestimation of the postcracking tensile strength in FRC members due to smaller final crack spacings and crack widths relative to those in conventionally reinforced concrete members. To investigate the effect of crack spacing on the accuracy of the FE simulations, Panel C1F1V3 was reanalyzed using three different crack spacings (2.25, 4.96, and 16.5 in. [57.2, 126, and 420 mm]). The crack spacing of 16.5 in. (420 mm) corresponded to the measured average crack spacing at first-cracking, and the crack spacing of 2.25 in. (57.2 mm) corresponded to the measured final average crack spacing. The results of the FE analysis are presented in Fig. 9.

The FE modeling relies on crack spacing parameters s_m to relate the average concrete principal tensile strain ϵ_{c1} to the crack width w_m through $w_m = \epsilon_{c1} \cdot s_m$. In calculating the average crack spacing, the following preliminary model was used

$$s_m = s_{mx} \cdot \cos^2 \theta_\sigma + s_{my} \cdot \sin^2 \theta_\sigma \qquad (6)$$
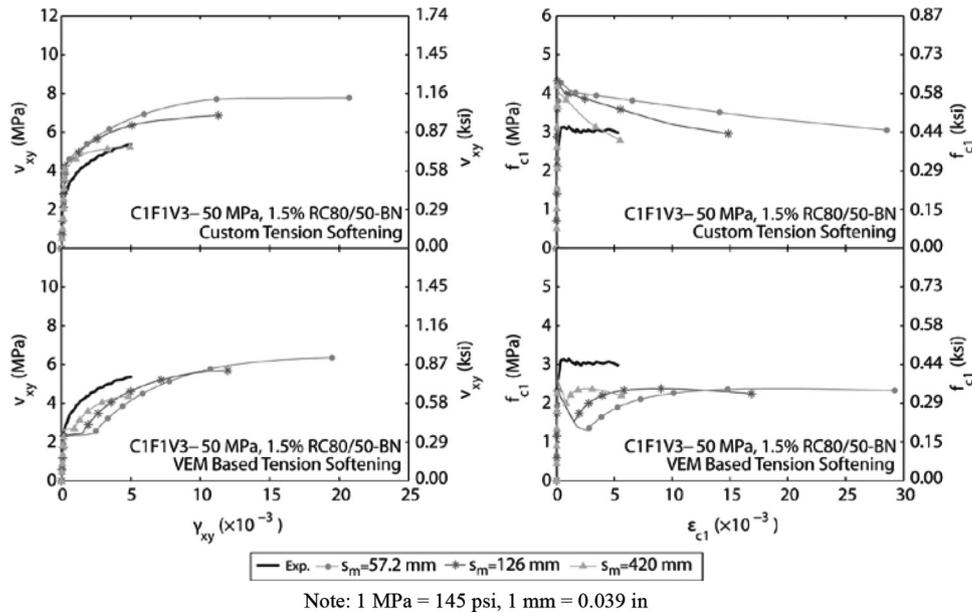
Note: 1 MPa = 145 psi, 1 mm = 0.039 in

Fig. 9—Effect of crack spacing on prediction of Panel C1F1V3.

$$s_{mx} = 2 \cdot \left(c + \frac{s_b}{10} \right) + \frac{k_1 \cdot k_2}{s_{mix}} \tag{7}$$

$$s_{mix} = \left[\sum_{i=1}^{n} \frac{\rho_{si}}{d_{bi}} \cdot \cos^2 \theta_{ni} \right] + K_{eff} \cdot \frac{V_f}{3 \cdot d_f} \tag{8}$$

$$s_{my} = 2 \cdot \left(c + \frac{s_b}{10} \right) + \frac{k_1 \cdot k_2}{s_{miy}} \tag{9}$$

$$s_{miy} = \left[\sum_{i=1}^{n} \frac{\rho_{si}}{d_{bi}} \cdot \sin^2 \theta_{ni} \right] + K_{eff} \cdot \frac{V_f}{3 \cdot d_f} \tag{10}$$

in which c is the clear concrete cover; s_b is the maximum spacing of the reinforcement ($s_b \not> 15 \times d_b$); $k_1 = 0.4$ (deformed bars) or 0.8 (plain bars); $k_2 = 0.25(\varepsilon_1 + \varepsilon_2)/(2 \times \varepsilon_1)$; ε_1 and ε_2 are the largest and smallest tensile strain within the effective embedment zone; θ_σ is the orientation of the principal stress field; and K_{eff} is fiber orientation factor (taken as 0.25).

When the custom tension-softening model was used, an increase in the crack spacing resulted in a wider crack, causing the concrete principal tensile stress to degrade at a faster rate, thus resulting in a reduction in the strength and deformation capacity of the panel. However, changing the crack spacing did not alter the failure mode of the panel as no crack slip was calculated. All analyses terminated due to the concrete principal compressive stress reaching the maximum compressive strength or due to inability to reach convergence because of very large crack width.

In the analyses using the VEM-based tension-softening model, an increase in the crack spacing also resulted in a wider crack, leading to the fibers being engaged sooner in carrying the tensile stress. This was reflected in the early strength gain of the panels analyzed using a large crack spacing, as indicated in Fig. 9. The increased crack spacing also resulted in a reduction in the strength and deformation capacity of the panels. Nevertheless, all analyses still terminated due to the concrete principal compressive stress reaching the maximum compressive stress or due to the inability to reach convergence.

Influence of crack slip consideration

In the context of the hybrid smeared rotating-crack concept employed by the DSFM, the calculation of crack shear slip using the Vecchio-Lai constitutive model[15] requires the presence of local shear stresses at the crack surface. However, for unreinforced elements, the DSFM will always predict zero shear stresses at the crack and, hence, crack stresses arising from the aggregate interlock mechanism are ignored and crack slip is considered nonexistent. This can result in an overestimation of the strength of the element, particularly when shear slip is critical. One way of addressing the presence of crack slip is to assume that a constant rotation lag between the principal stress field θ_σ and the principal strain field θ_ε exists.[3] The shear slip strain can then be determined using Mohr's circle, and the shear slip is taken as the largest of the values determined using the Vecchio-Lai model and the constant-rotation lag model. However, additional work is still required to evaluate the magnitude of rotation lag and shear slip in an FRC specimen.

SUMMARY AND CONCLUSIONS

Data from a series of FRC panel elements tested in pure shear were used to examine the constitutive responses of FRC with respect to compression softening, tension softening, and crack formation. The observed responses were then compared against the values obtained from commonly used corresponding constitutive models. The results of this investigation suggest the following conclusions:

1. The compression responses of the test panels agree with the accepted notion that the addition of fibers has little influence on the pre-peak compressive stress response of

concrete. However, the fibers were found to limit and control the coexisting transverse cracking and tensile straining, resulting in reduced compression softening of the concrete.

2. The tension responses of the control panels were governed by tension stiffening and were accurately modeled by the Vecchio-Collins 1982[9] tension-stiffening model. In contrast, the tension responses of the FRC panels were governed by tension softening. Attempts to model the response using VEM[4] resulted in a significant underestimation of the stiffness and strength of the principal tensile response of the panels. Thus, additional development of suitable tension-softening model for panels subjected to in-plane pure-shear loading is required.

3. Crack spacing parameters were found to significantly influence the prediction accuracy. As the crack spacings observed in the test panels showed significant progression through the course of loading, with the final spacings being significantly less than those at intermediate load stages, a model that can accurately present crack spacing progression is required to obtain an accurate representation of the tension response of the panels.

4. In the current implementation of the tension models of FRC, tension-softening behavior was found to govern the tensile behavior, but in a manner that results in no calculated shear stresses or shear slip on the crack surface. This results in over-prediction of the shear strength and deformation capacity of all FRC panels. Additional work is required to evaluate the shear slip on the crack surface of an FRC specimen.

NOTATION

$A_{c,eff}$	=	area of effective concrete embedment zone where steel reinforcement can influence crack widths
A_s	=	area of steel reinforcement
c	=	clear concrete cover
d_b	=	diameter of reinforcement steel
d_f	=	diameter of steel fibers
E_c	=	modulus of elasticity of concrete
f_c'	=	concrete compressive strength
f_{c1}	=	principal tensile stress of concrete
$f_{c1\text{-}fiber}$	=	postcracking tensile stress of concrete due to matrix
$f_{c1\text{-}matrix}$	=	postcracking tensile stress of concrete due to fibers
f_{c2}	=	principal compressive stress of concrete
$f_{c,base}$	=	compressive stress of concrete calculated using Popovics base curve
f_{cr}	=	concrete stress at onset of cracking
f_{res}	=	post-peak residual tensile strength of concrete
f_{sx}	=	average reinforcement stress in x-direction
f_{sy}	=	average reinforcement stress in y-direction
f_t'	=	tensile strength of plain concrete
f_{uf}	=	ultimate tensile strength of steel fibers
G_f	=	fracture energy
K_d	=	damage factor in VEM
K_{eff}	=	fiber orientation factor in Vector2
K_f	=	global orientation factor in VEM
k_1	=	coefficient characterizing bond properties of steel reinforcement
k_2	=	coefficient to account for strain gradient in concrete
l_f	=	length of steel fibers
s_b	=	maximum spacing of reinforcement ($s_b \ngtr 15 \times d_b$)
s_m	=	average crack spacing perpendicular to crack
s_{mix}	=	average crack spacing in x-direction for reinforcement in i-direction
s_{miy}	=	average crack spacing in y-direction for reinforcement in i-direction
s_{mx}	=	average crack spacing in x-direction
s_{my}	=	average crack spacing in y-direction
V_f	=	volume content of steel fibers
v_{ci}	=	local concrete shear stress at crack interface
v_u	=	maximum applied shear stress
v_{xy}	=	applied shear stress
w_m	=	average crack width
α	=	fiber engagement parameter in VEM
δ_s	=	shear slip
ε_1	=	largest tensile strain in effective embedment zone
ε_2	=	smallest tensile strain in effective embedment zone
ε_c'	=	concrete compressive strain corresponding to f_c'
ε_{ch}	=	characteristic strain of tensile softening curve (where $f_{c1}=0$)
ε_{cr}	=	concrete cracking strain
ε_{c1}	=	average principal net concrete axial tensile strain
ε_{c2}	=	average principal net concrete axial compressive strain
γ_u	=	shear strain corresponding to v_u
γ_{xy}	=	average shear strain
θ_n	=	angle between longitudinal axis of reinforcing bar and direction normal to crack
θ_ε	=	orientation angle of principal strain field, measured counterclockwise from x-axis
θ_σ	=	orientation of principal stress field, measured counterclockwise from x-axis
ρ_{eff}	=	$A_s/A_{c,eff}$
ρ_s	=	steel reinforcement ratio
ρ_x	=	reinforcement ratio in x-direction
ρ_y	=	reinforcement ratio in y-direction
τ_b	=	interfacial shear stress between reinforcement and concrete matrix

REFERENCES

1. Susetyo, J., "Fiber Reinforcement for Shrinkage Crack Control in Prestressed, Precast Segmental Bridges," PhD thesis, University of Toronto, Toronto, ON, Canada, 2009, 502 pp.

2. Susetyo, J.; Vecchio, F. J.; and Gauvreau, P., "Effectiveness of Steel Fiber as Minimum Shear Reinforcement," *ACI Structural Journal*, V. 108, No. 4, July-Aug. 2011, pp. 488-496.

3. Vecchio, F. J., "Disturbed Stress Field Model for Reinforced Concrete: Formulation," *Journal of Structural Engineering*, ASCE, V. 126, No. 9, 2000, pp. 1071-1077.

4. Voo, J. Y. L., and Foster, S. J., "Variable Engagement Model for Fiber Reinforced Concrete in Tension," *UNICIV Report No. R-420*, University of New South Wales, Sydney, Australia, June 2003, pp. 1-86.

5. Collins, M. P., and Porasz, A., "Shear Design for High Strength Concrete," *Proceedings of the Workshop on Design Aspects of High Strength Concrete*, V. 193, Comité Euro-International du Béton Bulletin d'Information, Paris, France, 1989, pp. 77-83.

6. Hsu, L. S., and Hsu, C. T. T., "Stress-Strain Behavior of Steel-Fiber High-Strength Concrete under Compression," *ACI Structural Journal*, V. 91, No. 4, July-Aug. 1994, pp. 448-457.

7. Naaman, A. E., and Homrich, J. R., "Properties of High-Strength Fiber Reinforced Concrete," *High-Strength Concrete*, SP-87, H. G. Russell, ed., American Concrete Institute, Farmington Hills, MI, 1985, pp. 233-249.

8. Vecchio, F. J., and Collins, M. P., "Compression Response of Cracked Reinforced Concrete," *Journal of Structural Engineering*, ASCE, V. 119, No. 2, Dec. 1993, pp. 3590-3610.

9. Vecchio, F. J., and Collins, M. P., "The Modified Compression Field Theory for Reinforced Concrete Elements Subject to Shear," ACI JOURNAL, *Proceedings* V. 83, No. 2, Mar.-Apr. 1986, pp. 219-231.

10. Wong, P. S., and Vecchio, F. J., "VecTor2 & FormWorks User's Manual," University of Toronto, Toronto, ON, Canada, Aug. 2002, 213 pp.

11. Dupont, D., and Vandewalle, L., "Calculation of Crack Widths with the σ-ε Method," *Test and Design Methods for Steel Fiber Reinforced Concrete: Background and Experiences—Proceedings of the RILEM TC162-TDF Workshop*, RILEM Technical Committee 162-TDF, Bochum, Germany, 2003, pp. 119-144.

12. ENV 1992-1-1, "Eurocode 2: Design of Concrete Structures—Part 1.1: General Rules and Rules for Buildings," 1991, 226 pp.

13. Moffatt, K., "Analyse de Dalles de Pont avec Armature Réduite et Béton de Fibres Métalliques," MScA thesis, École Polytechnique de Montréal, Montreal, QC, Canada, 248 pp.

14. Vecchio, F. J., VecTor2: Nonlinear Finite Element Analysis Program, 1995.

15. Vecchio, F. J., and Lai, D., "Crack Shear-Slip in Reinforced Concrete Elements," *Journal of Advanced Concrete Technology*, V. 2, No. 3, Oct. 2004, pp. 289-300.

NOTES: